Statistical study of parallel-dominated broadband 1-10 Hz waves in the auroral region

A. Olsson [a,*], P. Janhunen [b] H. Laakso [c] A. Vaivads [a]

[a] *Swedish Institute of Space Physics, Uppsala Division, Uppsala, Sweden*

[b] *Finnish Meteorological Institute, Geophysical Research, Helsinki, Finland*

[c] *ESTEC, Space Science Department, Noordwijk, The Netherlands*

Abstract

Broadband electrostatic noise (BEN) wave bursts are known to exist in the auroral region. Here we study the 1-10 Hz part of BEN statistically using Polar electric field observations from 1996-2000 in the altitude range 5000-30000 km. Mostly BEN electric wave fields are perpendicular to the magnetic field, but in this paper we concentrate on parallel-dominated waves, i.e. cases where the parallel component is a significant fraction of or larger than the perpendicular component. We find that the parallel-dominated waves have a preferred geocentric distance of ~ 3 Earth radii. This is an interesting result especially because the same altitude has recently found to be "magical" with respect to many other auroral acceleration related parametres also. We study the altitude profile under different nightside MLT, Kp and footpoint solar illumination conditions, as well as in MLT-ILAT and ILAT-R planes, where R is the geocentric distance. We discuss the possibility that the parallel-dominated waves could be ion-acoustic waves generated by ion beams or oscillating auroral potential structures and cavities.

Key words: Broadband electrostatic noise, auroral region, auroral acceleration

* Corresponding author.

Email addresses: ao@irfu.se (A. Olsson), pekka.janhunen@fmi.fi (P. Janhunen), hlaakso@rssd.esa.int (H. Laakso), andris.vaivads@irfu.se (A. Vaivads).

1 Introduction

Broadband electrostatic noise (BEN) was identified on auroral field lines using Hawkeye 1 and IMP 6 with quite large altitude coverage except for a data gap between 1.8 and 4 R_E geocentric distance (Gurnett and Frank, 1977; Lakhina et al., 2000). Gurnett and Frank (1977) pointed out that BEN is correlated with simultaneous ionospheric inverted-V electron precipitation and suggested that BEN might play a role in the heating and acceleration of auroral particles. They also reported that BEN is most intense in the 10-50 Hz frequency range and that in this frequency range, it is the strongest magnetospheric emission (Gurnett, 1991). Later it was remarked that BEN emissions are most intense below 1 Hz and decrease monotonically up to frequencies of several kilohertz (André, 1997).

Effects of BEN on particle acceleration have been investigated theoretically by Ashour-Abdalla and Thorne (1978) and its possible generation mechanisms by Lakhina (1993) and Mourenas and Krasnoselskikh (1993). BEN in the magnetotail has been studied in detail using ISEE-1 and Geotail (Grabbe, 1989; Matsumoto et al., 1994). The Geotail data suggest that BEN in the magnetotail and above 24 Hz consists of electrostatic solitary waves, perhaps driven by electron beams (Matsumoto et al., 1994). See also Grabbe (2000) for recent theoretical developments. From low-altitude Freja data it has been reported that some of the broadband electrostatic waves up to the ion plasma frequency are ion acoustic waves with typical parallel and perpendicular amplitudes of a few mV/m, but larger amplitudes are also possible (Wahlund, et al., 1994; André, 1997).

2 Observations

The wave electric fields in the 1-10 Hz frequency range are observed by the Polar Electric Field Investigation (EFI) instrument (Harvey et al., 1995). Using the Polar Plasma Wave Instrument (PWI) is not feasible in this study because PWI failed in 1997 before Polar was covering the altitude range which is the most interesting in this study. EFI measures the 3-D electric field with a sampling rate of 20 or 40 samples per second. In this study we do not use the spin-axis component of the measurement to avoid possible problems caused by the short boom length there (7 m). The spin axis of Polar is in the east-west direction so the magnetic field is usually close to the spin plane when Polar is above the auroral zone.

The Polar Magnetic Field Experiment (MFE) (Russell et al., 1995) is needed to decompose EFI data into parallel and perpendicular components. This makes it possible to obtain an estimate of the parallel wave electric field. We use the spin resolution (6 s) data from MFE.

3 Data processing

We took Level-0 EFI data, assumed E56= 0 (the fixed boom aligned with the spin axis and directed approximately azimuthally with respect to the dipole field), and expressed the electric field in GSE coordinates. Using spin-resolution (6 s) MFE data, the EFI electric field was decomposed into parallel and perpendicular components. The components were then bandpass-filtered in the 1-10 Hz frequency window. A running average with 12-second time resolution was then taken of the absolute value of the filtered time series of both components. We denote these average wave amplitudes by $E_{||}$ and $E_{\perp}$ and express them in mV/m. The motivation for filtering out frequencies below 1 Hz is to remain free of periodic signals that are due to harmonic multiples of the satellite spin (the spin period is 6 s). The motivation for the upper bound (10 Hz) is that the sampling rate in normal mode is 20 s^{-1} so 10 Hz corresponds to its Nyquist frequency.

Since the spin-axis component of the electric field was assumed to be zero, the perpendicular wave amplitudes used in the study are only $1/\sqrt{2}$ of the true values if the wave amplitudes are equally distributed in the plane perpendicular to the magnetic field. Thus the relative intensities of the parallel and perpendicular components discussed in this paper must be taken with this possible caveat in mind.

When doing the analysis we must assume that the wavelength is much longer than the probe separation (100 m). We now consider the justification of this assumption. If the wavelength would be only 100 meters, already the frequency due to the satellite motion alone would be about 30 Hz which is outside our 1-10 Hz frequency range, since the satellite speed in the region studied is at least about 3 km/s. So our 1 and 10 Hz waves correspond to at least 3 km and 300 m wavelengths, respectively. Thus, from the satellite motion argument we can conclude that at least in the frequency range 1-3 Hz the assumption of long wavelength is definitely justified. For the range 3-10 Hz there could in theory be some contamination due to short wavelength, but even this is unlikely since the satellite speed is most of the time 4-6 km/s (not 3 km/s) and because in addition to the satellite motion, the ambient plasma motion also introduces a comparable frequency component and also, furthermore, the waves probably have a nonzero phase velocity in the rest frame of the plasma.

The following data intervals were removed before doing the analysis:

(1) Days with no MFE data, because then one cannot separate parallel and perpendicular EFI wave electric field.
(2) Some data around EFI data gaps to avoid spurious spectral signals due to stepwise changed at data gap boundaries.
(3) Events where the angle between **B** and spin plane (spin angle) is larger than 6 degrees to avoid contamination of the parallel wave field by the perpendicular one. At 6 degrees and assuming approximate isotropy in the perpendicular plane the contamination is 10 %, which is much smaller than the parallel-dominated criterion of 40% (discussed and defined below).
(4) Events where the spin angle is smaller than 2 degrees, to avoid wake effects (one or several probes moves through the spacecraft's field-aligned wake).
(5) As mentioned earlier, only the frequency range 1-10 Hz is considered.

4 Specific event

To get a more concrete picture of the phenomena under investigation, we study in more detail an event that occurred on April 17, 1999. Notice, however, that a full understanding of the physical phenomenon (in particular, the question of the underlying wave mode) in an individual event like this is not possible with the available data. In Figure 1 panel a shows the parallel (red) and perpendicular (green) wave amplitudes filtered in 1-10 Hz frequency range and averaged over 12 s. Panels b and c are the perpendicular and parallel EFI spectrograms, respectively. The frequency range 1-10 Hz is marked with a black double-headed arrow in panels b and c. The main wave activity in this frequency range occurs 05:24-05:28 UT. The satellite arrives into the auroral region from the polar cap at $\sim$ 05:21 UT.

The 12 s averaged wave amplitudes are rather small (usually some mV/m). The waves are typically bursty and consequently the instantaneous values can be significantly larger than the 12 s averaged ones. As an example, Figure 2 shows an interval of high-pass filtered instantaneous observations of waves occurring in Figure 1. The peak parallel wave amplitudes exceed 10 mV/m in a time series where the frequencies smaller than 1 Hz have been removed. Furthermore, in this event the parallel wave field is on the average as large as the perpendicular one. Usually the perpendicular fields are larger than the parallel ones, but the focus of this paper is to consider cases where the parallel field is significant.

5 Statistical results

5.1 Identification of parallel waves

The identification of waves having a significant parallel component requires some care, because the perpendicular component is usually much larger and slightly non-optimal orientation of the booms causes a "leaking" of the perpendicular wave power to the parallel one, which easily masks the real parallel wave components when doing statistics. To get around this problem we first identify epochs where the parallel component $E_{||}$ is significant in comparison to the perpendicular $E_{\perp}$ as a 12-s average. We parametrise this as the condition $E_{||} \geq sE_{\perp}$ where s is a given parameter (the slope) that we set beforehand. We also require that the parallel component itself is significant, $E_{||} \geq E_{||}^{\mathrm{thr}}$ where $E_{||}^{\mathrm{thr}}$ is a given threshold.

In Figure 3 we show the effects of s and $E_{||}^{\mathrm{thr}}$ on the occurrence frequency of having $E_{||}$ larger than $sE_{\perp}$ and $E_{||}^{\mathrm{thr}}$. Each of the six subplots has a different slope value, while the three panels in the subplot correspond to different thresholds $E_{||}^{\mathrm{thr}}$. The invariant latitude (ILAT) range is 65-74. Each panel presents statistics for low Kp (Kp≤ 2, blue lines), high Kp (Kp> 2, red lines) and all Kp (black lines). The error bars have been calculated from the assumption that all datapoints within one auroral crossing are correlated: the relative error shown is $1/\sqrt{M}$ where M is the number of different orbital crossings where at least one datapoint exceeds the given threshold. This is probably an overestimation of the errors. If the relative error is more than 50% for the black curve (all Kp), the black curve is shown alone without error bars and without Kp separation. For zero slope (top left subplot in Figure 3) only the threshold $E_{||}^{\mathrm{thr}}$ is effective, and the decreasing trend with altitude likely reflects the fact that the perpendicular fields decrease in amplitude with altitude (because of the flux tube scaling possibly together with other effects) and the parallel fields seen here are mostly due to "leakage" from the perpendicular fields. However, when a nonzero slope is introduced, an intriguing phenomenon gradually emerges: near 3 R_E geocentric distance waves with a significant parallel component appear. This feature becomes increasingly clearer as the slope is increased and as the threshold is made higher, although eventually the growth of the statistical error makes the feature more difficult to discern (bottom right subplot).

To study this feature further, one can use almost any slope/threshold combination displayed in Figure 3 apart from the trivial zero slope case; the result is qualitatively independent of the selection of the slope and the threshold. The slope and the threshold have an effect on how clearly the preferred altitude is seen and how large the statistical errors are. As a useful compromise, we adopt the value $s = 0.4$ for the slope and $E_{\|}^{\mathrm{thr}} = 0.1$ mV/m for the threshold.

Since there is a preferred altitude for parallel-dominated waves, it is natural to ask if there is any similar pattern for the perpendicular-dominated waves. In Figure 4 we show the parallel-dominated waves in the left subplot (because $s = 0.4$ and $E_{\|}^{\mathrm{thr}} = 0.1$ mV/m, this subplot is identical with the second panel of the top right subplot of Figure 3) and the corresponding perpendicular-dominated waves in the right subplot. The top panel shows the orbital coverage in hours. The perpendicular-dominated wave occurrence frequency in the right panel of Figure 4 gives the probability that $E_{\|} < 0.4E_{\perp}$ and $E_{\perp} \geq 1$ mV/m. We see that the perpendicular-dominated waves do not have a preferred altitude, but decay with altitude rather uniformly. This is likely due to the expansion of flux tubes with distance which reduces the perpendicular electric fields. Further discussion of the perpendicular-dominated waves is outside the scope of this paper.

5.2 MLT dependence

In Figure 5 we investigate the occurrence frequency of parallel-dominated waves decomposed into the three different nightside magnetic local time (MLT) sectors 18-22, 22-02 and 02-06. Apart from the division into different MLTs this plot is similar to the left subplot of Figure 4. All MLT sectors display very similar characteristics, except that in the morning MLT sector the overall occurrence frequency is smaller than in the evening and midnight sectors. In the evening sector the occurrence frequency peaks at one bin (0.5 R_E) higher than in the other MLT sectors, which is probably due to the fact that the $\sim 3R_E$ evening sector maps more often to the sunlit ionosphere than to the dark ionosphere (for solar illumination dependence, see subsection 4.2.5 below).

5.3 Kp dependence

In Figures 3-5, the observations have been divided into two Kp ranges so that blue is used for low Kp (0-2), red for high Kp (> 2) and black for all Kp's. There is not much different between the low and high Kp results, but the occurrence frequency is generally slightly larger for high Kp than for low Kp. When looking at the plots, having low and high Kp visible separately has also the benefit of providing a rough idea of the magnitude of the statistical error, an idea which is independent of the displayed error bars and the assumptions underlying them.

5.4 Solar illumination dependence

The parallel-dominated wave statistics are decomposed according to whether the satellite's footpoint in the ionosphere is sunlit or in darkness; the results are shown in Figure 6. The peak occurrence frequency appears at $2.75 R_E$ geocentric distance in darkness and at $3.25 R_E$ geocentric distance in sunlit conditions. As was remarked above, because the evening sector has mainly sunlit coverage, this is the likely reason why in the evening sector the peak occurs at higher altitude than in other MLT sectors.

5.5 ILAT dependence

The bottom panel of Figure 7 shows the occurrence frequency of parallel-dominated waves in the MLT-ILAT (invariant latitude) plane, the top panel being the corresponding orbital coverage. Measurements from all geocentric distances below 6 R_E are taken into account in this plot. The definition of the occurrence frequency is the same as e.g. in Figure 5, i.e. $E_{||}$ must be larger than $0.4 E_{\perp}$ and also larger than 0.1 mV/m. We see that the occurrence frequency mostly increases towards higher ILAT and that the region of high occurrence frequencies extends to the lowest ILAT in the midnight MLT sector. At least qualitatively, constant occurrence frequency contours follow the average auroral oval, which is well known to reside at lowest ILAT in the midnight sector. Figure 7 suggests that the peak occurrence rates occur in the poleward edge of the oval in the premidnight sector.

In Figure 8 we show the distribution of the occurrence frequency in the ILAT-R plane (R is the geocentric distance), for all measurements in the nightside (18-06 MLT). Again, the top panel is the orbital coverage and the bottom panel is the occurrence frequency itself. In this representation, both the preferential geocentric distance of $\sim 3 R_E$, already seen in many figures in the present paper, and the tendency of the occurrence frequency to increase towards higher ILAT are clear. One can also see from Figure 8 that the preferential geocentric distance tends to rise with increasing ILAT and becomes less sharply defined at high altitudes.

We also remark that the occurrence frequency in Figure 8 appears anticorrelated with the orbital coverage, which at first glance might suggest an error in data processing. However, we have checked in many ways that there is no such error; e.g. if one decomposes the plot in different Kp indices, the anticorrelation almost disappears. Thus the apparent anticorrelation in this plot is only a coincidence.

5.6 Correlation with plasma density

To find out if the parallel-dominated waves are measured because of increased Debye length due to very small plasma density, we computed the rank correlation coefficient between the occurrence of parallel-dominated waves and the plasma density estimated from the spacecraft potential. The rank correlation coefficient is slightly positive ($\sim 10 - 20$ %) at all altitudes, indicating that parallel-dominated waves are slightly more common when the plasma density is higher. In other words, the parallel-dominated fields do not usually occur within auroral cavities. Thus our observations cannot be explained by the Debye length becoming too large compared with the boom length.

6 Summary and discussion

In this paper we have investigated the 1-10 Hz electric wave component in the auroral zone statistically, using observations from the EFI instrument onboard the Polar satellite. We first summarise our main findings and then discuss the most interesting points in more detail.

(1) Parallel-dominated waves tend to occur at a preferred geocentric distance of $\sim 3R_E$ (Figure 4, left subplot). Perpendicular-dominated waves do not follow this pattern, but their occurrence frequency decreases smoothly with altitude (Figure 4, right subplot).
(2) The preferred geocentric distance of parallel-dominated waves is 2.75 R_E when the ionospheric footpoint is in darkness, but moves to 3.25 R_E when it is sunlit (Figure 6).
(3) The occurrence frequency of parallel-dominated waves is generally slightly larger for high Kp than for low Kp index, but otherwise no significant difference can be discerned.
(4) In MLT-ILAT plane, constant occurrence frequency contours follow at least qualitatively the average auroral oval, so the parallel-dominated waves likely have something to do with auroral processes. However, they are not centred at the mean oval but rather at the poleward edge of the oval. This needs not, however, be a real effect but may be due to masking by stronger perpendicular BEN fields, which are the most common within the central auroral zone: when perpendicular wave fields are strong, one cannot reliably detect weak underlying parallel fields.

The statistical results do not tell directly what is the physical wave mode responsible for the detected parallel-dominated signals. Usually in space physics one first tries to understand individual events and only then moves to statistical studies. Here, however, this approach cannot be followed since we are dealing with a new, hitherto unobserved phenomenon, while the available data do not allow for a direct identification of the wave mode (the PWI instrument was no longer working when Polar covered the most relevant altitude range). Thus, we think that doing a statistical study before fully understanding the individual events is quite justified in this case.

One possibility for generating parallel wave fields in the auroral oval can be kinetic Alfvén waves that may break up when entering the $\sim 3R_E$ geocentric distance from above (Kletzing, 1994) and thus developing a significant parallel component. By waves breaking up we mean a process where a single wave breaks into several daughter waves with smaller perpendicular wavelength. However, this mechanism would probably produce parallel wave components that are still small compared to the simultaneously occurring perpendicular ones, although they could be significant in the absolute sense. It may well be that Alfvén wave associated parallel wave fields exist in the auroral region, but we cannot reliably detect them with the method used in this paper. Thus our observations most likely cannot be explained by kinetic Alfvén waves.

Ion acoustic waves are electrostatic modes that may also be parallel-dominated, depending on the generation mechanism and on the propagation conditions. They can be generated at least by multi-component ion beams by the fan instability (Vaivads et al., 1995). How quickly they are damped when propagating depends crucially on the temperatures of different electron and ion populations. Ion acoustic wave propagation is possible in many angles with respect to the magnetic field, thus the waves are not confined to the flux tube where they are generated. At least in some events, the parallel-dominated waves are seen slightly before and after Polar enters a region of strong perpendicular wave activity. The ion acoustic waves may be generated at the flux tubes where the strongest activity occurs, but measuring them is possible only when strong in situ perpendicular waves are not masking them. This is in accordance with the abovementioned result that the parallel-dominated waves have a small positive correlation with plasma density because strong perpendicular fields that would mask the ion acoustic waves are less common in denser plasma. Explaining our results in terms of ion acoustic waves therefore seems possible.

In conclusion, the existence of parallel-dominated waves predominantly near 3 R_E geocentric distance is the most important result of this paper. The parallel-dominated waves are statistically a persistent feature which occurs in all nightside MLT sectors in both low and high Kp. What makes this result particularly interesting is that the geocentric distance where the parallel wave power peaks ($\sim 3R_E$) has recently been found to be “magical” with respect to many parameters related to auroral processes: it contains peak occurrence frequencies of density cavities (Janhunen et al., 2002), potential minima and perpendicular electric fields (Janhunen et al., 2003a) and upgoing ion beams (Janhunen et al., 2003b); see Olsson and Janhunen (2003) for a recent review. An explanation of the parallel-dominated waves as ion-acoustic waves radiating from the "epicentre" of auroral energy transfer is compatible with these results, since the region with the strongest density cavities and electric fields is likely to radiate ion acoustic waves the most efficiently. A further observational study of the "magic" $3 - 3.5 R_E$ geocentric distance range in general, and the parallel-dominated waves in particular, is complicated by the fact that the satellite data coverage of this altitude is much less than at altitudes both above and below it.

Acknowledgements. We thank F.S. Mozer and C.T. Russell for providing the EFI and MFE data, respectively. The work of AO was supported by the Swedish Research Council and that of PJ by the Academy of Finland.

References

André, M., Waves and wave-particle interactions in the auroral region, *J. Atmos. Sol. Terr. Phys., 59,* 1687–1712, 1997.

Ashour-Abdalla, M., and R.M. Thorne, Toward a unified view of diffuse auroral precipitation, *J. Geophys. Res., 83,* 4755–4766, 1978.

component observed by the Freja spacecraft: Artifacts or real

Grabbe, C., Wave propagation effects of broadband electrostatic noise in the magnetotail, *J. Geophys. Res., 94,* 17299–17304, 1989.

Grabbe, C., Generation of broadband electrostatic waves in Earth's magnetotail, *Phys. Rev. Lett.,* 84, 3614–3617, 2000.

Gurnett, D.A. and L.A. Frank, A region of intense plasma wave turbulence on auroral field lines, *J. Geophys. Res., 82,* 1031–1050, 1977.

Gurnett, D.A., Auroral plasma waves, pp. 241–254, in *Auroral physics,* edited by C.-I. Meng, M.J. Rycroft and L.A. Frank, Cambridge, 1991.

Harvey, P., F.S. Mozer, D. Pankow, J. Wygant, N.C. Maynard, H. Singer, W. Sullivan, P.B. Anderson, R. Pfaff, T. Aggson, A. Pedersen, C.G. Falthammar and P. Tanskanen, The electric field instrument on the polar satellite, Space Science Reviews 71, 583-596, 1995.

Janhunen, P., A. Olsson and H. Laakso, Altitude dependence of plasma density in the auroral zone, *Ann. Geophysicae,* 20, 1743–1750, 2002.

Janhunen, P. and A. Olsson, The occurrence frequency of auroral potential structures and electric fields as a function of altitude using Polar/EFI data, *Ann. Geophysicae,* in press, 2003a.

Janhunen, P., A. Olsson and W.K. Peterson The occurrence frequency of upward ion beams in the auroral zone as a function of altitude using Polar/TIMAS and DE-1/EICS data, *Ann. Geophysicae,* in press, 2003b.

Kletzing, C.A., Electron acceleration by kinetic Alfvén waves, *J. Geophys. Res., 99,* 11095–11103, 1994.

Lakhina, G.S., Generation of low-frequency electric field fluctuations on the auroral field lines, *Ann. Geophys., 11,* 705–710, 1993.

Lakhina, G.S., B.T. Tsurutani, H. Kojima and H. Matsumoto, “Broadband” plasma waves in the boundary layers, *J. Geophys. Res., 105,* 27791–27831, 2000.

Matsumoto, H., H. Kojima, T. Miyatake, Y. Omura, M. Okada, I. Nagano and M. Tsutsui, Electrostatic solitary waves (ESW) in the magnetotail: BEN wave forms observed by GEOTAIL, *J. Geophys. Res., 21,* 2915–2918, 1994.

Mourenas, D. and V. Krasnoselskikh, A numerical study of instabilities producing auroral broadband electrostatic bursts, *Ann. Geophys., 11,* 711–716, 1993.

Olsson, A. and P. Janhunen, Some recent developments in understanding auroral electron acceleration processes, *IEEE Trans. Plasma Sci.,* in press, 2003.

Russell, C.T., R.C. Snare, J.D. Means, D. Pierce, D. Dearborn, M. Larson, G. Barr and G. Le, The GGS/Polar Magnetic Fields Investigation, *Space Sci. Rev.,* 71, 563–582, 1995.

Vaivads, A., K. Rönnmark and M. André, Generation of ion acoustic waves by fan instability, *J. Geophys. Res., 100,* 19435–19440, 1995.

Wahlund, J.-E., P. Louarn, T. Chust, H. de Feraudy, A. Roux, B. Holback, P.O. Dovner and G. Holmgren, On ion acoustic turbulence and the nonlinear evolution of kinetic Alfvén waves in aurora, *Geophys. Res. Lett., 21,* 1831–1834, 1994.

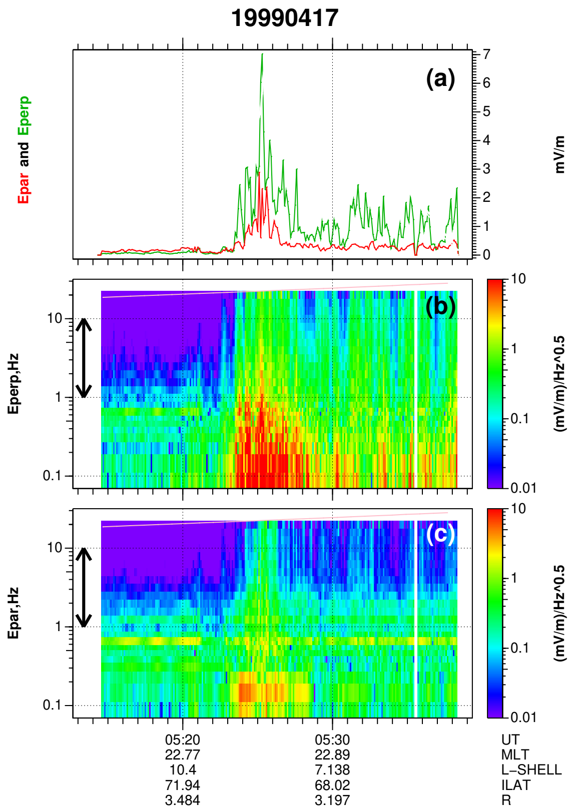

Fig. 1. Electric field measurements during Polar auroral crossing on 17 April 1999, 05:15-05:38 UT. Parallel (red) and perpendicular (green) wave power in 1-10 Hz range averaged over 12 s (panel a), perpendicular wave spectrogram (panel b), parallel wave spectrogram (panel c).

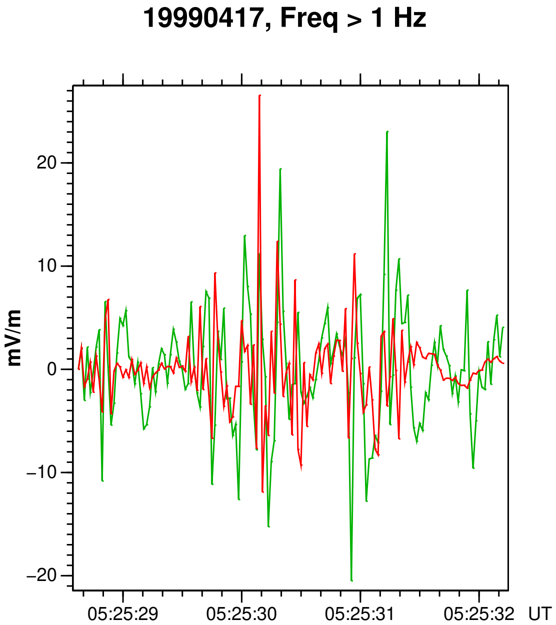

Fig. 2. High-resolution wave data during the 1999/04/17 event displaying parallel (red) and perpendicular (green) electric field component time series, with frequencies smaller than 1 Hz filtered away. The excerpt starts at 05:25:28.6 UT, lasting for 3.6 seconds.

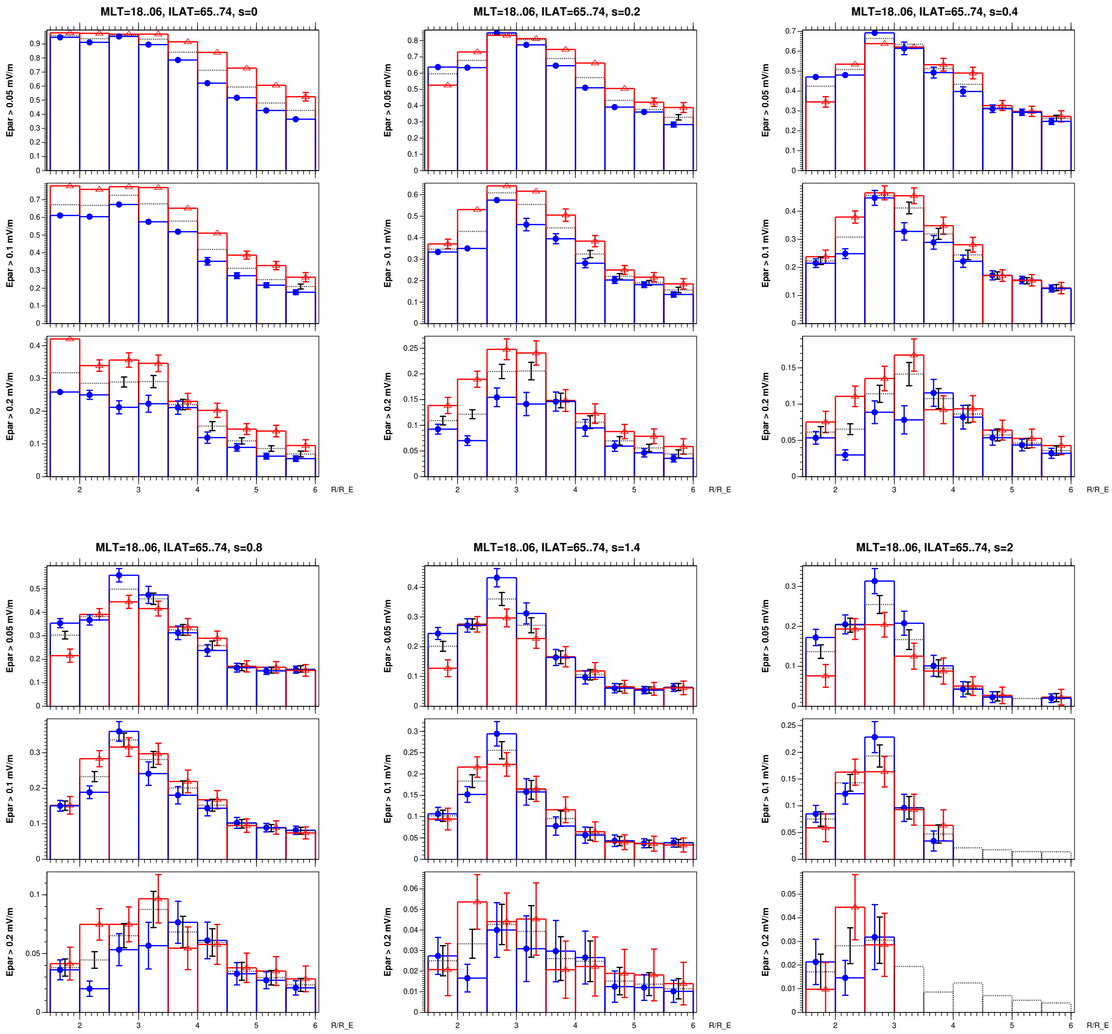

Fig. 3. Occurrence frequency of parallel-dominated waves for different slopes (s) and thresholds ($E_{||}^{\mathrm{thr}}$). Each of the six subplots corresponds to one slope s in $E_{||} \geq sE_{\perp}$, where s is 0, 0.2, 0.4, 0.8, 1.4 and 2.0. Each subplot contains three panels, corresponding from top to bottom to $E_{||}^{\mathrm{thr}}$ of 0.05, 0.1 and 0.2 mV/m. Red lines are for high Kp (Kp > 2), blue for low Kp (Kp ≤ 2) and black for all Kp's. If the all-Kp relative error is more than 50%, the black curve is shown alone without error bars and without blue and red curves (bottomleft subplot).

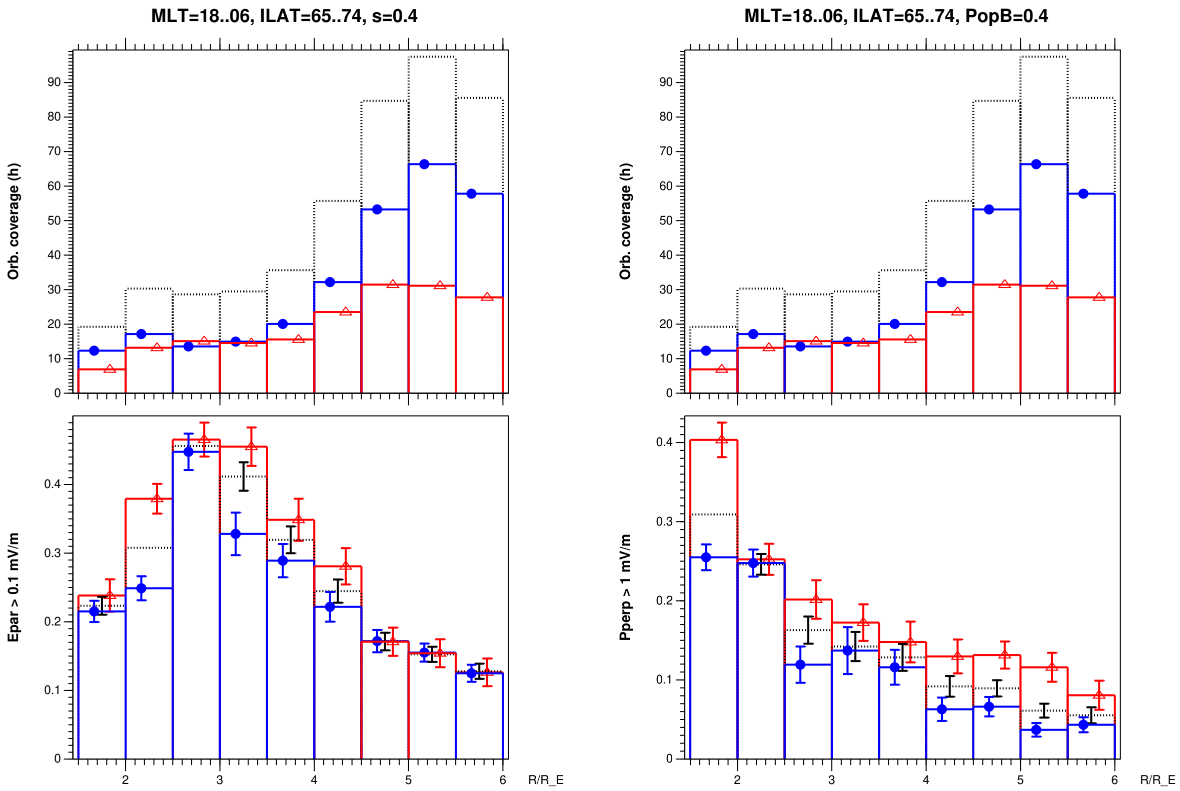

Fig. 4. Parallel-dominated waves (left) and perpendicular-dominated waves (right). Top panel is instrumental coverage in hours and bottom panel is the occurrence frequency of parallel-dominated waves where $E_{||} \geq 0.4E_{\perp}$ and $E_{||} \geq 0.1$ mV/m (left), and perpendicular-dominated waves where $E_{||} < 0.4E_{\perp}$ and $E_{\perp} \geq 1$ mV/m (right). Colours and error bars as in Figure 3.

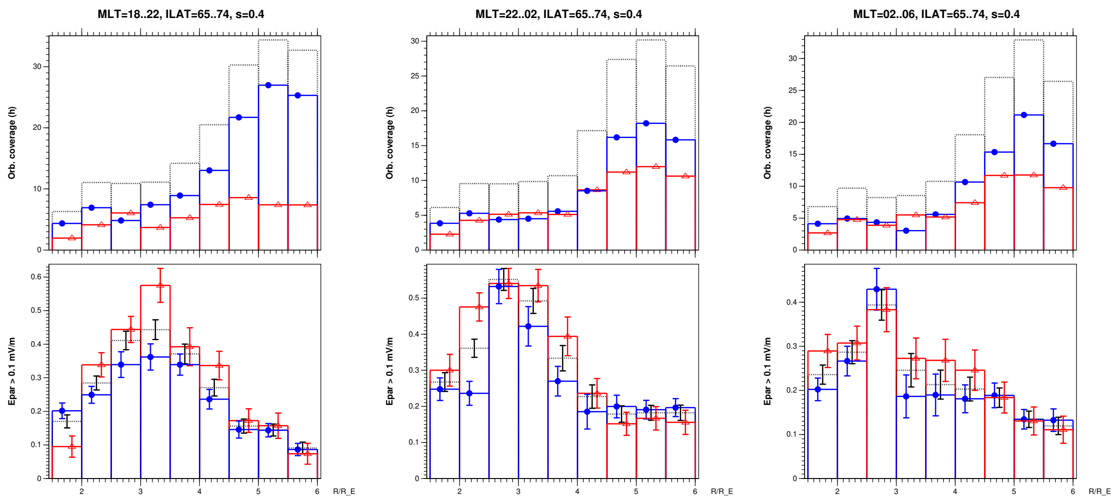

Fig. 5. Same as left panel (i.e., parallel-dominated waves) of Figure 4 but separated into three nightside MLT sectors.

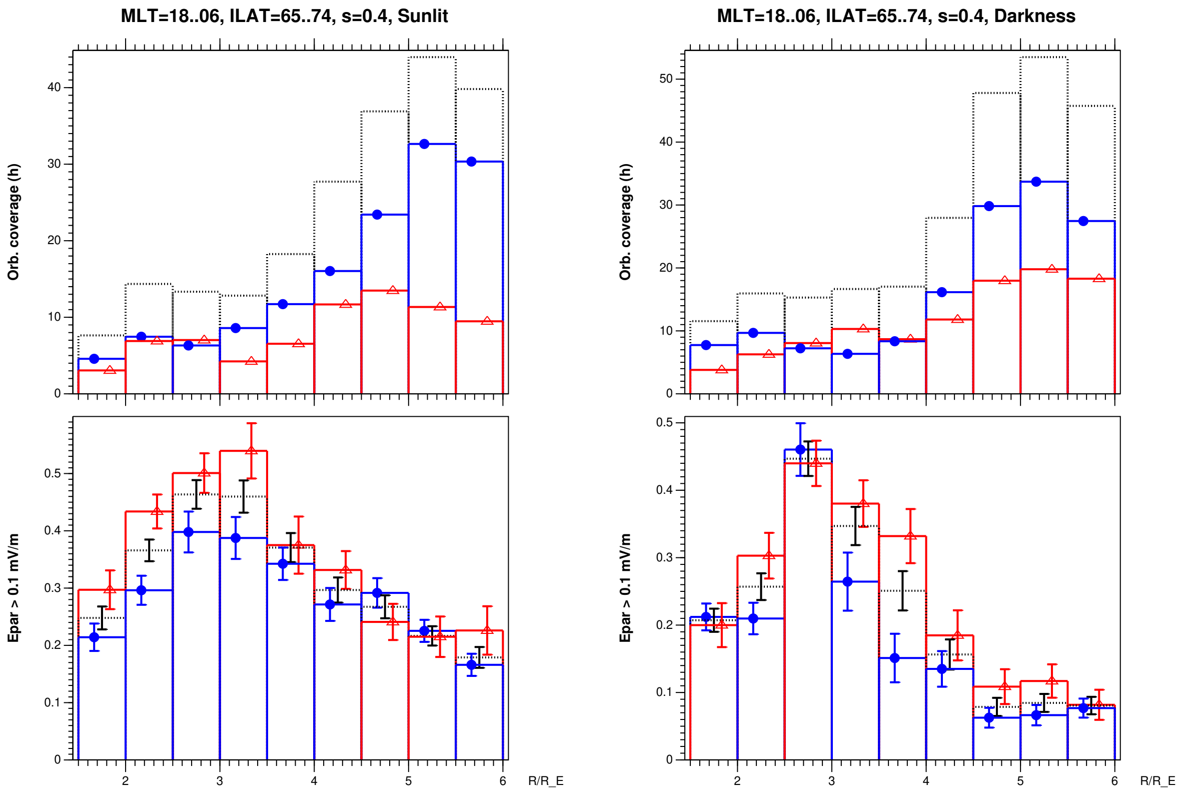

Fig. 6. Occurrence of parallel-dominated waves under different solar illumination conditions. Same as the left panels (i.e., parallel-dominated waves) of Figure 4 but the measurements are decomposed into two cases depending upon whether the satellite footpoint in the ionosphere is sunlit (left panel) or in darkness (right panel).

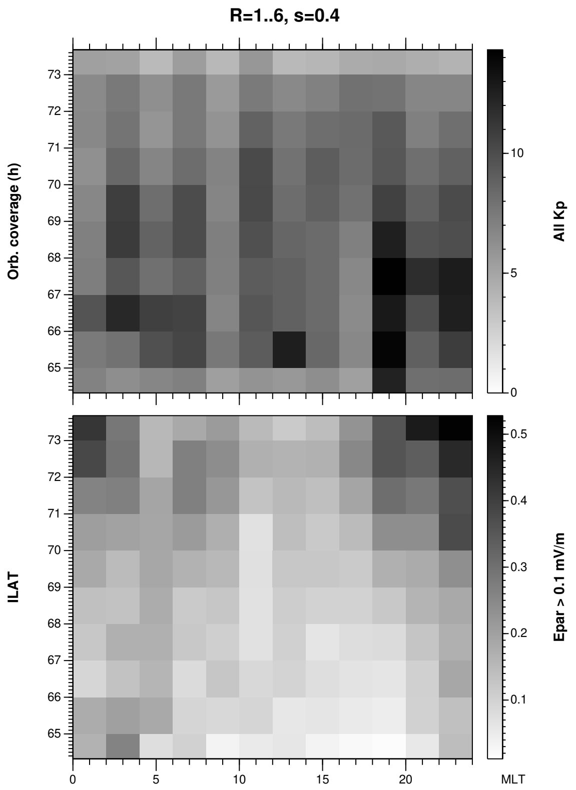

Fig. 7. Occurrence of parallel-dominated waves in the MLT-ILAT plane. Statistics contain measurements from all distances below 6 R_E. Top panel is orbital coverage in hours and bottom panel is the occurrence frequency for $E_{\|} \geq 0.4 E_{\perp}$ and $E_{\|} \geq 0.1$ mV/m.

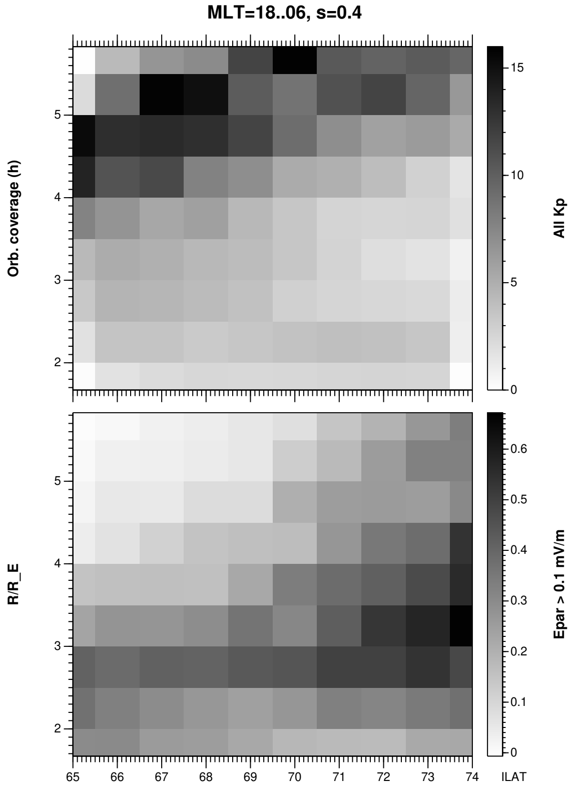

Fig. 8. Occurrence of parallel-dominated waves in the ILAT-R plane for the nightside sector (18-06 MLT). Top panel is orbital coverage in hours and bottom panel is the occurrence frequency for $E_{\|} \geq 0.4 E_{\perp}$ and $E_{\|} \geq 0.1$ mV/m.